Progress In Electromagnetics Research, PIER 87, 131–147, 2008

DESIGN AND ANALYSIS OF PHASED ANTENNA ARRAY WITH LOW SIDELOBE BY FAST ALGORITHM

T. Yuan, N. Yuan, L.-W. Li, and M.-S. Leong

Department of Electrical and Computer Engineering
The National University of Singapore
10 Kent Ridge Crescent, 119260, Singapore

Abstract—In this paper, a high performance phased antenna array is designed. Compared with the traditional ones, this antenna array has a lower sidelobe characteristic of down to $-16\,\mathrm{dB}$. At different scanning angles, the comparison between calculated and measured results of S-parameters and E- and H-plane antenna patterns is made and a very good agreement is found. Moreover, the precorrected fast Fourier transform method is employed to accelerate the entire computational process to reduce significantly both the memory requirement and computational time, but to increase the design accuracy and optimization efficiency.

1. INTRODUCTION

Phased array antennas have found increasing applications in radar engineering and, more recently, in satellite and cellular communications. In the most recent applications, smart antennas play an important role in cellular base stations. Despite of increasing popularity, the optimum designs and practical fabrications of planar phased array antennas with low sidelobe level and narrow beamwidth remains a challenging task [1].

The most commonly used method for reducing the sidelobe levels of a uniform array involves amplitude tapering, in which the excitation amplitudes of the array elements generally decrease with the distance from the center of the array. Several techniques were developed [2, 3] for obtaining amplitude shading coefficients for a linear array of uniformly spaced point sources, and they produce the narrowest possible beam for a given degree of uniform minor lobe suppression. However, the two major consequences are the reduction of the sidelobe levels and the broadening of the beamwidths. These two phenomena are always

complementary to each other. Since the beamwidth is widened, the directivity of the array decreases. If a lower sidelobe level is needed, then a wider beamwidth must be accepted as a compromise. A significant effort has been so spent as to find amplitude distributions that minimize the beamwidth for a given sidelobe level or optimize the pattern in some other ways [4].

There are several methods of analysis for such antenna arrays. The most popular approaches are the transmission-line method, cavity approach, and full-wave integral equation techniques including primarily the boundary element method and the method of moments (MoM) [5]. When applied properly, in general, the full-wave models are more practical and accurate. In recent years, the spatial-domain method of moments has been extensively used to solve the mixed potential integral equation (MPIE) for the design and optimization of microstrip structures [6, 7]. Although the method is robust, the solution procedure of the resultant matrix equation requires $O(N^3)$ operations if the Gaussian elimination is used; or $O(N^2)$ operations per iteration if an iterative method is used, where N is the number of unknowns. So in the modeling of the electrically large phased antenna array, computational limitations can be easily exceeded.

One of the powerful techniques that can significantly reduce the memory requirement and computing time is the precorrected fast Fourier transform (pFFT) method which was first proposed by Philips and White [8] to solve Laplacian equations in electrostatic problems. It was later extended further to solve Helmholtz equations in electromagnetic problems in radio frequency [9 10]. The precorrected-FFT method has been further developed by Yuan et al. [11] analyzing scattering by, and radiation of, large microstrip antenna arrays; and by Nie et al. [9, 10, 12] solving scattering problems of arbitrarily shaped objects based on the surface integral equations and volume integral equations [13–15]. As a further application, a high performance phased antenna array is designed in this paper. Compared with the traditional array with uniform dimension elements, this type of antenna array has a lower sidelobe characteristic.

In this present work, we present an accurate and efficient method combined the pFFT algorithm to analyze the proposed phased antenna array. The mixed-potential integral equation is discretized and employed for the efficient computation, where the Rao-Wilton-Glisson (RWG) basis functions are chosen for the method of moments procedure and the discrete complex image method [16] is applied to obtain the closed form Green's function. Finally, we use the precorrected-FFT method to accelerate the solution of the matrix equation and reduce the memory and computational requirements to

$O(N)$ and $O(N \log N)$, respectively. Both calculated and experimental results of return loss (S-parameter), radiation patterns, and phase-shift angles of the proposed arrays are obtained and compared. A very good agreement between calculated and measured results of such arrays has been obtained.

2. DESIGN PROCEDURE

2.1. Series-fed Taper Antenna Array Design

The seven-element series-fed taper microstrip antenna array is shown in Fig. 1(a), which was used as the starting point of this work. The array is designed to resonate at 10 GHz. The dielectric substrate of the microstrip array has a relative dielectric constant of 2.2 and thickness of 31 mil.

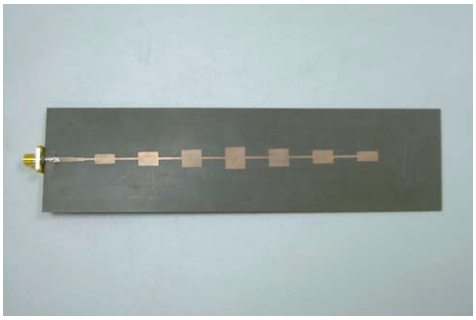

(a)

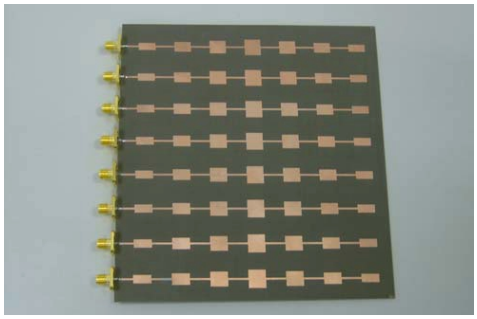

(b)

Figure 1. Photographs of the antenna arrays, (a) the 1×7 single series-fed taper antenna array, (b) the 8×7 series-fed taper antenna array.

An array with a uniform excitation usually produces the narrowest possible beamwidth along with the highest sidelobe level. High sidelobes can increase interference or result in spurious signal reception. Therefore, it is necessary to reduce the sidelobe levels. To achieve the objective, a taper in the amplitudes of the elements is proposed.

As mentioned in [4], it is considered a linear taper distribution for the proposed antenna array. An amplitude varies linearly from a peak value of 1 at the array center to a value of C ($-6\,\mathrm{dB}$) at the edge, which is shown in Fig. 2. a_n is the amplitude of the nth element, it can be obtained by

$$a_n = C + (1 - C)\left[1 - \frac{2z_n}{L}\right] \tag{1}$$

The array element conductance (g_n) is proportional the amplitude coefficient (a_n) squared and the input conductance to the array (g_{in}) which is the sum of all the elements conductances is normalized [4].

$$g_{in} = \sum_{n=1}^{N} g_n = \sum_{n=1}^{N} K a_n^2 = 1 \tag{2}$$

where K is the constant of proportionality. From Eq. (1) and Eq. (2), when the array element number is determined, the required elements conductances can be found and the theoretical width of the array element then can be finally obtained [5]. Since each width and length of the array element is obtained based on the theoretical calculation, it is usually different between practical results. Some errors may make the main beam direction deviate to the proposed one. Also the sidelobe is different with the calculated value. Then it is better to optimize the width and length values of the antenna array by simulation. Here an accurate and efficient method combined the pFFT algorithm is used to analyze the purposed phased antenna array.

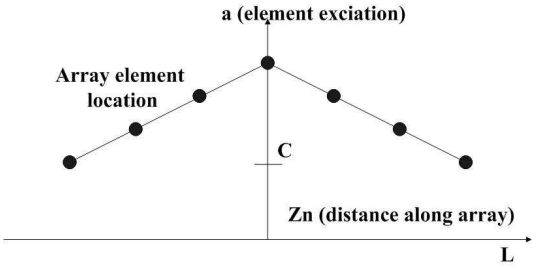

Figure 2. Linear tapered distribution.

When tapering the amplitude distributions, the highest excitation should be located at the center of the array and then it decreases toward the edges [4]. If the array has an odd number of elements, then the center element has the largest excitation. For an even number of array elements, the two elements adjacent to each other located in the center share the largest excitation.

With end-fed arrays, the elements nearest the feed will couple only a small amount of power and therefore must be fairly narrow in width. The feed line must be small as compared to the narrowest patch. In this case, a 80-Ω line will be used, and it is a 1.111-mm wide line that is considerably smaller than the rectangular patch width.

Two-dimensional arrays are designed as shown in Fig. 1(b), being composed with eight single series-fed taper arrays. The element spacing is chosen as $2/3\lambda_0$ which can be used to prevent grating lobes.

2.2. Implementation of Phased Shift

As shown in Fig. 3, a RF signal is emitted by antennas through the feeding network and phase shifter. By adjusting the phase shifter, the radiation pattern in H-plane could be continuously steered over a range of angles and the beam-scanning function of the phased array can be achieved.

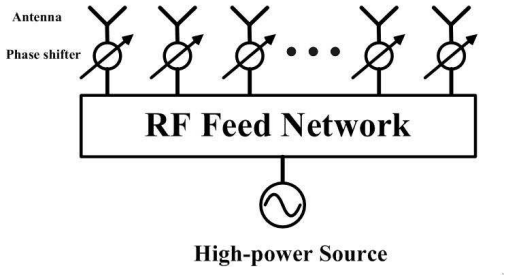

Figure 3. Block diagram of the phased-array system.

3. FORMULATION

In this section, we first briefly introduce the mixed-potential integral equation formulation using the closed-form multilayered Green's functions derived efficiently from the discrete complex image method. For the solution of the mixed-potential integral equation, the method of moments with triangular patches and a set of basis functions as

described in [17] is used and accelerated by the pFFT algorithm, for analyzing the proposed antenna array. Finally, we briefly explain how to calculate radiation patterns and extract S-parameters to be presented in this paper.

3.1. Dyadic Green's Functions for 3-D Planar Multilayered Medium

Consider an arbitrarily shaped object embedded in a planar multilayered medium, and excited by arbitrary currents distribution $(\boldsymbol{J}, \boldsymbol{M})$, as shown in Fig. 4. The fields due to these sources may be expressed as mixed potential forms

$$\boldsymbol{E} = -j\omega\mu_0 \left\langle \overline{\boldsymbol{G}}^{AJ}, \boldsymbol{J} \right\rangle + \frac{1}{j\omega\epsilon_0} \nabla \left\langle G^{VJ}, \nabla' \cdot \boldsymbol{J} \right\rangle + \left\langle \overline{\boldsymbol{G}}^{EM}, \boldsymbol{M} \right\rangle \quad (3a)$$

$$\boldsymbol{H} = -j\omega\epsilon_0 \left\langle \overline{\boldsymbol{G}}^{AM}, \boldsymbol{M} \right\rangle + \frac{1}{j\omega\mu_0} \nabla \left\langle G^{VM}, \nabla' \cdot \boldsymbol{M} \right\rangle + \left\langle \overline{\boldsymbol{G}}^{HJ}, \boldsymbol{J} \right\rangle \quad (3b)$$

where, $\overline{\boldsymbol{G}}^{AJ/AM}$ are the dyadic Green's functions for magnetic and electric vector potentials. $G^{VJ/VM}$ are the Green's functions for corresponding electric and magnetic scalar potentials and $\overline{\boldsymbol{G}}^{EM/HJ}$ are the dyadic Green's functions for coupled field, respectively. Here, the time harmonic fields with the $e^{j\omega t}$ time dependence is assumed.

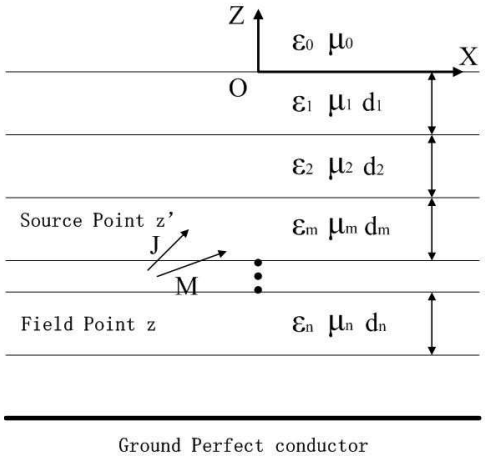

Figure 4. Planar multilayered medium with source and field points located in layers m and n, respectively.

All of the Green's functions for the vector and scalar potentials are not uniquely defined in multilayered media. To derive the general forms of the Green's functions, the detailed discussion in Michalski-Zheng's C-formulation shows that it is preferable to choose $\overline{\boldsymbol{G}}^{AJ/AM}$ as

$$\overline{\boldsymbol{G}}^{AJ/AM} = = \begin{pmatrix} G_{xx}^{AJ/AM} & 0 & G_{xz}^{AJ/AM} \\ 0 & G_{xx}^{AJ/AM} & G_{yz}^{AJ/AM} \\ G_{zx}^{AJ/AM} & G_{zy}^{AJ/AM} & G_{zz}^{AJ/AM} \end{pmatrix} \tag{4}$$

and $G^{VJ/VM}$ are expressed as the scalar potential for a horizontal electric dipole and a horizontal magnetic dipole, respectively.

The $\overline{\boldsymbol{G}}^{EM/HJ}$ can be obtained by the curl of the $\overline{\boldsymbol{G}}^{AJ/AM}$ as

$$\overline{\boldsymbol{G}}^{EM/HJ} = \begin{pmatrix} G_{xx}^{EM/HJ} & G_{xy}^{EM/HJ} & G_{xz}^{EM/HJ} \\ G_{yx}^{EM/HJ} & G_{yy}^{EM/HJ} & G_{yz}^{EM/HJ} \\ G_{zx}^{EM/HJ} & G_{zy}^{EM/HJ} & 0 \end{pmatrix}. \tag{5}$$

In general, the Green's functions for a multilayered medium are expressed in terms of Sommerfeld integrals, which can be written as

$$\boldsymbol{G}(\boldsymbol{r}, \boldsymbol{r'}) = \frac{1}{2\pi} \int_0^\infty \widetilde{G}\left(k_\rho; z, z'\right) J_n\left(k_\rho \rho\right) k_\rho^{n+1} dk_\rho \tag{6}$$

where $\widetilde{G}$ denotes the counterpart of spectral domain Green's function $\boldsymbol{G}(\boldsymbol{r})$, $J_n(\bullet)$ stands for the first kind cylindrical Bessel function of order n, $k_\rho = \sqrt{k_x^2 + k_y^2}$, and $\rho = \sqrt{(x-x')^2 + (y-y')^2}$.

Because the proposed antenna array forms a 2-dimensional structure, only the G_{xx}^{AJ} and G^{VJ} components are used in the design procedure. More detailed description of the above procedure can be found in [18] and will not be addressed further in this paper.

3.2. Method of Moments

For the solution to the mixed-potential integral equation in (3), the method of moments with triangular discretization is used and the Rao-Wilton-Glisson basis functions [17] are considered in the discretization. The basis functions belonging to a common edge n of two triangular

patches T_n^+ and T_n^- are defined [17] as

$$\boldsymbol{f}_n(\boldsymbol{r}) = \begin{cases} \dfrac{\boldsymbol{\rho}_n^+(\boldsymbol{r})}{2A_n^+}, & \boldsymbol{r} \quad \text{in} \quad T_n^+; \\ \dfrac{\boldsymbol{\rho}_n^-(\boldsymbol{r})}{2A_n^-}, & \boldsymbol{r} \quad \text{in} \quad T_n^-; \\ 0, & \text{otherwise.} \end{cases} \tag{7}$$

The notations $A_n^{\pm}$ represent the areas of the triangles of $T_n^{\pm}$. The vectors $\boldsymbol{\rho}_n^{\pm}(\boldsymbol{r})$ are defined as $\pm(\boldsymbol{r} - \boldsymbol{r}_n^{\pm})$ if $\boldsymbol{r}$ is in $T_n^{\pm}$, where the vectors $\boldsymbol{r}_n^{\pm}$ denote the position vectors of the free vertices of the triangle pair.

In the method of moments procedure, we assume the following expansion of $\boldsymbol{J}$ in terms of the basis functions

$$\boldsymbol{J}(\boldsymbol{r}) = \sum_{n=1}^{N} I_n \boldsymbol{f}_n(\boldsymbol{r}) \tag{8}$$

for the surface-current density on S. Using the Galerkin's method and applying the 2-dimensional divergence theorem, we obtain the following matrix equation

$$\overline{\boldsymbol{Z}} \cdot \boldsymbol{I} = \boldsymbol{V}. \tag{9}$$

The system matrix of $\overline{\boldsymbol{Z}}$ is referred to as *impedance* matrix, the vector $\boldsymbol{V}$ is called *excitation* or *voltage vector*, and the unknown vector to be solved for is $\boldsymbol{I}$. The elements of the impedance matrix $\overline{\boldsymbol{Z}}$ and the voltage vector $\boldsymbol{V}$ are given by

$$\begin{aligned} Z_{i,j} = {} & j\omega\mu_0 \int_{T_i}\int_{T_j} \boldsymbol{f}_i(\boldsymbol{r}) \cdot \overline{\boldsymbol{G}}^{AJ}\left(\boldsymbol{r}, \boldsymbol{r'}\right) \cdot \boldsymbol{f}_j\left(\boldsymbol{r'}\right) d\boldsymbol{r'} d\boldsymbol{r} \\ & + \frac{1}{j\omega\epsilon_0} \int_{T_i}\int_{T_j} \boldsymbol{\nabla} \cdot \boldsymbol{f}_i(\boldsymbol{r}) \cdot \boldsymbol{\nabla'} \cdot \boldsymbol{f}_j\left(\boldsymbol{r'}\right) \cdot G^{VJ}\left(\boldsymbol{r}, \boldsymbol{r'}\right) d\boldsymbol{r'} d\boldsymbol{r} \end{aligned} \tag{10}$$

and

$$V_i = \int_{T_i} \boldsymbol{f}_i(\boldsymbol{r}) \cdot \left[\boldsymbol{E}^i(\boldsymbol{r}) + \boldsymbol{E}^r(\boldsymbol{r})\right] d\boldsymbol{r} \tag{11}$$

where $\boldsymbol{f}_i$ and $\boldsymbol{f}_j$ represent the testing and basis functions, and T_i and T_j denote their supports respectively. $\boldsymbol{E}^i(\boldsymbol{r})$ and $\boldsymbol{E}^r(\boldsymbol{r})$ are the incident field and reflected field, respectively. For arbitrarily shaped, conducting or penetrable objects embedded in a multilayered medium,

the dyadic Green's function for the vector potential in the spatial domain can be expressed as

$$\begin{aligned}\overline{\boldsymbol{G}}^{AJ} &= G_{xx}^{AJ}\left(\widehat{\boldsymbol{x}}\widehat{\boldsymbol{x}}+\widehat{\boldsymbol{y}}\widehat{\boldsymbol{y}}\right)+G_{xz}^{AJ}\widehat{\boldsymbol{x}}\widehat{\boldsymbol{z}}+G_{yz}^{AJ}\widehat{\boldsymbol{y}}\widehat{\boldsymbol{z}} \\ &\quad +G_{zx}^{AJ}\widehat{\boldsymbol{z}}\widehat{\boldsymbol{x}}+G_{zy}^{AJ}\widehat{\boldsymbol{z}}\widehat{\boldsymbol{y}}+G_{zz}^{AJ}\widehat{\boldsymbol{z}}\widehat{\boldsymbol{z}}. \end{aligned} \tag{12}$$

3.3. The Precorrected-FFT Solution to the MPIE

As shown in (9), a numerical solution to the matrix equation in the method of moments requires $O(N^3)$ operations and $O(N^2)$ memory to store the matrix elements, where N is the number of unknowns. The large operation number and memory requirement render the method of moments solution for the large-scaled phased arrays of printed dipoles prohibitively expensive. Therefore, the precorrected-FFT method is used here to speed up the matrix-vector multiplication and to improve the efficiency of iterative procedure in the method of moments.

Like other fast algorithms, the precorrected-FFT algorithm also works on the approximation of the far-zone interactions. The acceleration of the solution to the equation in (9) is accomplished by filling only an order of N subsets in $\boldsymbol{Z}$ and computing the voltage vector $\boldsymbol{V}$ in two parts, that is,

$$\boldsymbol{V} = \overline{\boldsymbol{Z}}_{\text{near}} \cdot \boldsymbol{I}_{\text{near}} + \boldsymbol{V}_{\text{far}} \tag{13}$$

where $\overline{\boldsymbol{Z}}_{\text{near}}$ is sparse and contains only the entries associated with elements within a threshold distance, and $\boldsymbol{V}_{\text{far}}$ represents the far-zone interactions based on the uniform grids and computed by an approximation technique.

Application of the precorrected-FFT algorithm requires that the whole geometry be enclosed in a regular rectangular grid. However, for the planar phased arrays of printed dipoles, it is only necessary to employ a planar uniform grid that can be coincident with the original triangular grid [11]. Then the matrix-vector multiplication can be approximated in a four-step procedure given below:

- to project the element singularity distributions to point singularities on the uniform rectangular grids;
- to compute the potentials at the grid points, due to the grid sources by FFT-accelerated convolutions;
- to interpolate the grid point potentials onto the triangular elements within a certain cell; and
- to add the precorrected direct near-zone interactions finally.

The detailed procedure can be obtained in [11].

Because of the large number of elements in planar arrays of practical interest and of the computational complexity, it is imperative that attention be given to the efficient calculation of Eq. (9). As mentioned previously, the numerical solution to the matrix equation in the method of moments requires $O(N^3)$ operations and $O(N^2)$ memory to store the matrix elements. These requirements may exceed the memory available and will render the method computationally intractable. Therefore, the precorrected-FFT method is used to reduce the memory and computational requirements to $O(N)$ and $O(N \log N)$, respectively. For increasing the efficiency of the iterative solution, the generalized conjugate residual method (GCR) is used to solve the matrix equation for fast convergence.

3.4. Treatment of the S-parameters Extraction and Far-Field Calculation

The scattered or radiated field in the far-field zone can be evaluated conveniently using the reciprocity theorem. In this approach, the radiated field in the direction of (θ, ϕ) can be evaluated as

$$\begin{pmatrix} \boldsymbol{E}_{\theta}^{rad}(\boldsymbol{r}) \\ \boldsymbol{E}_{\phi}^{rad}(\boldsymbol{r}) \end{pmatrix} = -\frac{j\omega\mu_0 e^{-jk_0 r}}{4\pi r} \iint_S \boldsymbol{J}(\boldsymbol{r'}) \cdot \begin{pmatrix} \boldsymbol{E}_{\theta}(\boldsymbol{r'}) \\ \boldsymbol{E}_{\phi}(\boldsymbol{r'}) \end{pmatrix} dr' \qquad (14)$$

where $\boldsymbol{E}_{\theta}(\boldsymbol{r})$ and $\boldsymbol{E}_{\phi}(\boldsymbol{r})$ denote the fields in the presence of the dielectric substrate without the microstrips produced by the θ- and ϕ-polarized electric current elements placed at the observation point in the far zone [19].

For the S-parameter extraction, we use the three-point curve-fitting scheme together with the precalculated characteristic impedance and propagation constant of the corresponding microstrip line [20].

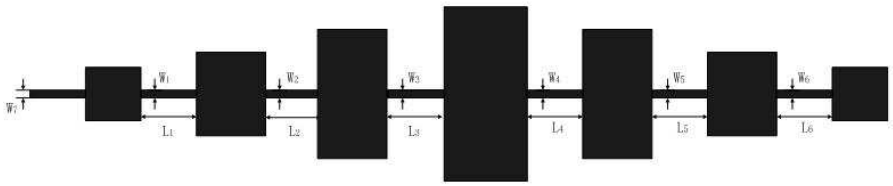

Figure 5. Configurations of the single antenna array.

4. RESULTS AND ANALYSIS

In this section, we demonstrate the proposed 1×7 (single seven-element) series-fed antenna array and the 8×7 (eight seven-element) series-fed phased arrays. Calculated results of radiation patterns, return loss, and gain of the arrays are shown and the experimental results show reasonable agreement with the simulation and high performance of the proposed antenna array.

Table 1. Array geometric parameters.

Size (mm) Element	Patch width	Patch length	Line width	Line length
1	4.8	10.133	1.11	11.12
2	6.55	9.93	1.11	11.12
3	8.385	9.787	1.11	11.12
4	10.35	9.682	1.11	11.12
5	8.385	9.787	1.11	11.12
6	6.55	9.93	1.11	11.12
7	4.8	10.133	1.11	—

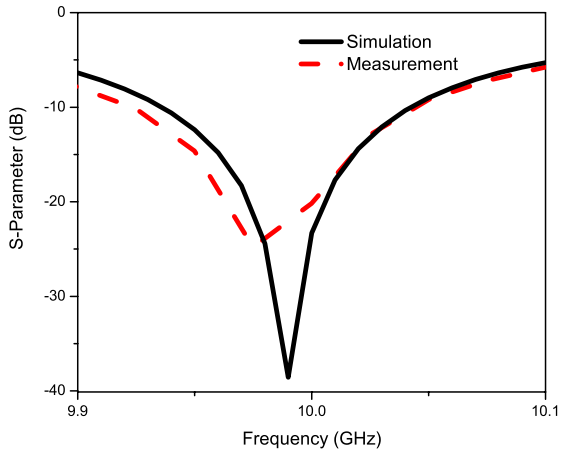

Figure 6. S-parameter, S_{11}, of the single series-fed taper antenna array.

To check the performance of this 8×7 phased antenna arrays, the single seven-element series-fed taper antenna array is first designed and analyzed (where the relative permittivity is assumed as $\epsilon_r = 2.2$, while the substrate thickness is $h = 31$ mil), as shown in Fig. 1(a). The series-fed taper antenna array is designed and shown in Fig. 5. The detailed geometrical parameters are listed in Table 1.

Figure 6 shows the magnitude of the scattering parameter, S_{11}. The E- and H-plane radiation patterns at 10 GHz of the single array are depicted in Fig. 7. Also the results are compared with the

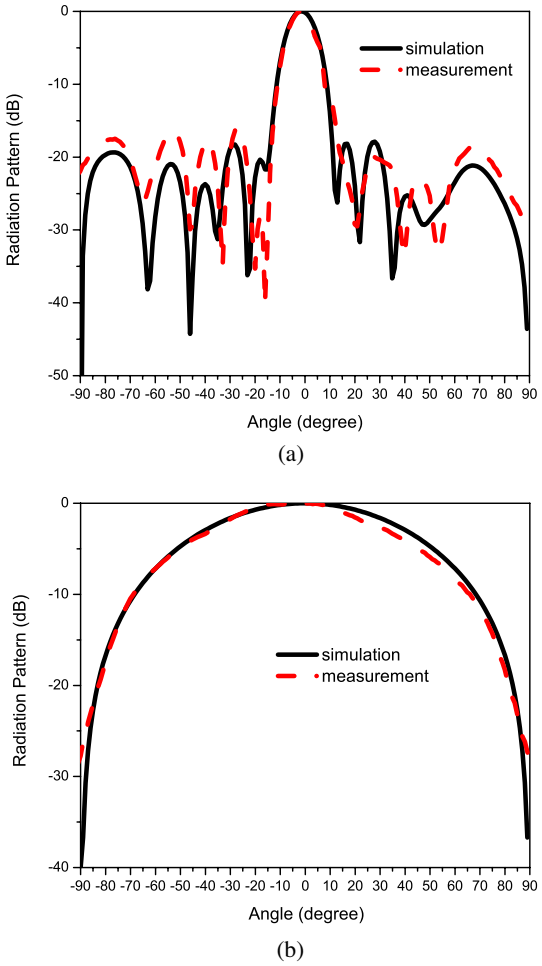

Figure 7. The radiation patterns of the single series-fed taper antenna array, (a) E-plane, (b) H-plane.

simulation data obtained using the method of moments accelerated with the pFFT fast algorithm. Because of the taper structure, E-plane of the proposed antenna array shows the low sidelobe characteristic. The relative sidelobe level of about -16 dB has been reduced by using the taper antenna array.

Figure 8 shows the measured patterns in both E- and H-planes when the phase shifters were adjusted to scan the beam to 0° (broadside), -7°, and 11°, respectively. In the E-plane, the radiation patterns are changed inconspicuously because no phase shift is involved. From the Fig. 8, for both E-plane and H-plane, it can be seen that the relative sidelobe level are both about -14 dB. The

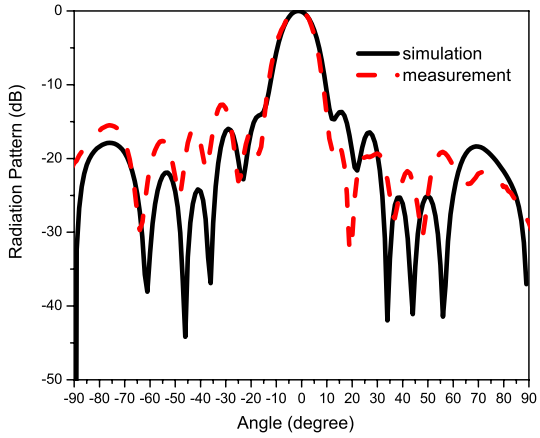

(a)

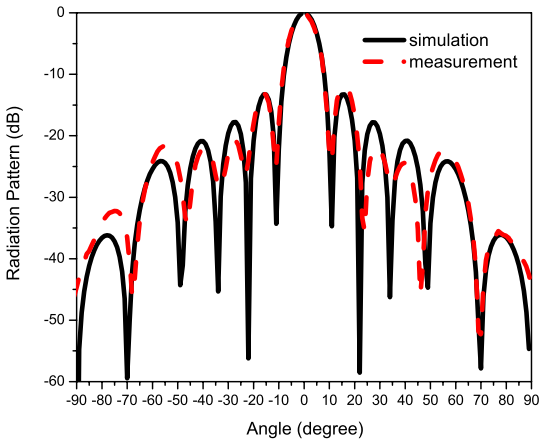

(b)

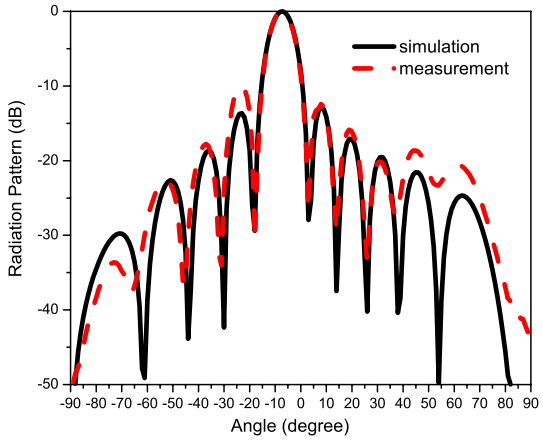

(c)

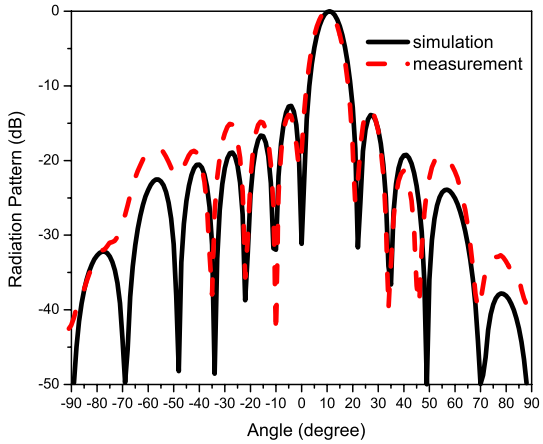

(d)

Figure 8. Radiation patterns of the antenna array at different scanning angles, (a) E-plane (Scanning angle = 0°), (b) H-plane (Scanning angle = 0°), (c) H-plane (Scanning angle = −7°), (d) H-plane (Scanning angle = 11°).

detail performance of the present antenna array are listed in Table 2. Without phased shifted, the beam direction is just 0° which is same with the simulation results. Also from the Fig. 8, it is seen that the comparison of shift angles between calculated and measured results is, in general, very good in agreement.

The computational resource requirements of the precorrected-FFT method are listed in Table 3. The residual error is 0.001. As can be seen, the pFFT requires 33.4 Mb of memory and the iteration number of 368 on a Pentium 2.4 G personal computer for the design of 8×7 phased antenna arrays.

Table 2. The performance of 8×7 series-fed taper antenna array.

Pattern	Gain (dBi)	Beamwidth (°)	Max cross-polarization (dBi)
E-plane	22.3	9	1.1
H-plane	21.7	10	2

Table 3. Computational requirements by the pFFT method.

Array	1×7	8×7
No of Triangles	2528	7520
No of Unknowns	3517	9816
MoM Memory (Mb)	99.8	755
pFFT Memory (Mb)	20.3	33.4
No. of Iterations	516	368

5. CONCLUSIONS

In this paper, a high performance phased antenna array is designed. Compared with the traditional one, this type of antenna arrays has a lower-level sidelobe characteristic. The sidelobe level is reduced by using the taper structures. For different scanning angles, the comparisons between calculated and measured results show very good agreements. Moreover, the precorrected fast Fourier transform method is employed to accelerate the entire computational process so as to reduce significantly both the memory requirement and computational time for large arrays. Very good agreements have been obtained between calculated and measured results of such arrays, namely, radiation patterns, return loss, and gain of the arrays.

ACKNOWLEDGMENT

Helpful discussion between the first author and Dr. Jian-Ying Li in Temasek Laboratories at the National University of Singapore is greatly appreciated. The project is partially supported by a joint project between the National University of Singapore and the Hitachi Cable Ltd., Tokyo, Japan.

REFERENCES

1. Dolph, C. L., "A current distribution for broadside arrays which optimizes the relationship between beamwidth and side-lobe level," *Proc. IRE*, Vol. 34, 335–348, June 1946.
2. Riblet, H. J., "Discussion on 'A current distribution for broadside arrays which optimizes the relationship between beamwidth and side-lobe level'," *Proc. IRE*, Vol. 35, 489–492, June 1947.
3. Pritchard, R. L., "Optimum directivity patterns for linear point arrays," *J. Acoust. Soc. Am.*, Vol. 25, 879–891, Sept. 1953.
4. Sainati, R. A., *CAD of Microstrip Antennas for Wireless Applications*, Artech House, Boston, London, 1996.
5. Balanis, C. A., *Antenna Theory Analysis and Design*, Wiley, New York, 1997.
6. Liu, Y.-X., L.-W. Li, T.-S. Yeo, and M.-S. Leong, "Automatic extraction of surface-wave poles and residuals of potential Green's functions for multilayered media," *IEE Proceedings on Microwave, Antennas and Propagation*, Vol. 151, No. 2, 463–469, 2004.
7. Liu, Y.-X., L.-W. Li, T.-S. Yeo, and M.-S. Leong, "Application of DCIM to MPIE-MoM analysis of 3-D PEC objects in multilayered media," *IEEE Transactions on Antennas and Propagation*, Vol. 50, No. 2, 157–162, 2002.
8. Phillips, J. R. and J. K. White, "A precorrected-FFT method for capacitance extraction of complicated 3-D structures," *Proc. Int. Conf. Computer-Aided Design*, Nov. 1994.
9. Yuan, N., T. S. Yeo, X. C. Nie, and L. W. Li, "Precorrected-FFT algorithm for solving combined field integral equations in electromagnetic scattering," *Journal of Electromagnetic Waves and Applications*, Vol. 16, No. 8, 1171–1187, Aug. 2002.
10. Nie, X. C., L. W. Li, N. Yuan, and T. S. Yeo, "Fast analysis of scattering by arbitrarily shaped three-dimensional objects using the precorrected-FFT method," *Microwave Opt. Technol. Lett.*, Vol. 34, No. 6, 438–442, Sept. 2002.
11. Yuan, N., T. S. Yeo, X. C. Nie, and L. W. Li, "A fast analysis

of scattering and radiation of large microstrip antenna arrays," *IEEE Transactions on Antennas and Propagation*, Vol. 51, No. 9, 2218–2216, Sept. 2003.

12. Nie, X. C., L. W. Li, N. Yuan, T. S. Yeo, and Y. B. Gan, "A fast analysis of electromagnetic scattering by arbitrarily shaped homogeneous dielectric objects," *Microwave Opt. Technol. Lett.*, Vol. 38, No. 1, 30–34, July 2003.
13. Nie, X. C., N. Yuan, L.-W. Li, Y. B. Gan, and T. S. Yeo, "A fast combined field volume integral equation solution to EM scattering by 3D dielectric objects of arbitrary permittivity and permeability," *IEEE Transactions on Antennas and Propagation*, Vol. 54, No. 3, 961–969, Mar. 2006.
14. Yuan, N., T. S. Yeo, X. C. Nie, Y. B. Gan, and L.-W. Li, "Analysis of probe-fed conformal microstrip antennas on finite ground plane and substrate," *IEEE Transactions on Antennas and Propagation*, Vol. 54, No. 2, 554–563, Feb. 2006.
15. Nie, X. C., Y. B. Gan, N. Yuan, C.-F. Wang, and L.-W. Li, "An efficient hybrid method for analysis of slot array enclosed by a large radome," *Journal of Electromagnetic Waves and Applications*, Vol. 20, No. 2, 249–264, Feb. 2006.
16. Fang, D. G., J. J. Yang, and G. Y. Delisle, "Discrete image theory for horizontal electric dipoles in a multilayered medium," *Proc. IEEE, Pt. H*, Vol. 135, No. 5, 297–303, Oct. 1988.
17. Rao, S. M., D. R. Wilton, and A. W. Glisson, "Electromagnetic scattering by surface of arbitrary shape," *IEEE Transactions on Antennas and Propagation*, Vol. 30, No. 5, 409–418, May 1982.
18. Zhang, M., L. Bai, T. Yuan, L.-W. Li, and Z.-S. Wu, "Analysis of multilayered millimeter wave structure with via-holes connected," *International Journal of Infrared and Millimeter Waves*, Vol. 26, No. 2, 315–327, Feb. 2005.
19. Wang, C. F. and F. Ling, "A fast full-wave analysis of scattering and radiation from large finite arrays of microstrip antennas," *IEEE Transactions on Antennas and Propagation*, Vol. 46, No. 10, 1467–1474, 1998.
20. Chang, D. C. and J. X. Zheng, "Electromagnetic modeling of passive circuit elements in MMIC's," *IEEE Transactions Microwave Theory Tech.*, Vol. 40, No. 9, 1741–1747, Sept. 1992.